Nonlinear transport in a two-dimensional electron gas with a periodically modulated potential

S. K. Lyo and W. Pan

Phys. Rev. B **84**, 195320 — Published 23 November 2011

DOI: 10.1103/PhysRevB.84.195320

Nonlinear Transport in a Two-dimensional Electron Gas with a Periodically Modulated Potential

S. K. Lyo*,† and W. Pan*

*Sandia National Laboratories, Albuquerque, NM 87185, USA

†Department of Physics and Astronomy, University of California, Irvine, CA, 92697

(Received:)

Abstract

We study the nonlinear response of the current of a two-dimensional electron gas with a periodically modulated potential in one direction in a strong DC electric field at low temperatures. The dependence of the current on the field, the electron density and the temperature is investigated by using a relaxation-time approximation for inelastic scattering. Elastic scattering is treated microscopically including interband scattering. The roles of elastic and inelastic scattering on the nonlinear current are examined. The result is applied to the Kronig-Penney model. It is found that, for a fixed total scattering rate, the field dependence of the current is insensitive to the ratio of the elastic and inelastic scattering rates in contrast with the recent results of the nonlinear current of similar models of a single mini-band in one dimension and three dimensions. The result from the Kronig-Penney model is compared with the recent data from a modulated two-dimensional GaAs quantum well which show evidence of the negative differential conductance.

PACS: 72.20.Ht, 73.63.Nm, 72.10.Bg

I. INTRODUCTION

An electron undergoes a periodic motion in a strong electric field F, sweeping the Brillouin zone of a periodic lattice with a frequency $f = peF/2\pi\hbar \equiv \omega_F/2\pi$, where ω_F is the angular speed and p is the lattice period. These so-called Bloch oscillations[1] are typically damped before the electrons sweep through the band because of scattering, reaching a steady state and yielding the negative differential conductance. In a superlattice with a large period, the Bloch frequency f can fall in a terahertz region under a moderate field. This fascinating phenomenon has received much attention in the past for its potential to yield terahertz generation, detection, and also for applications to negative differential conductance.[2–18] Investigations of Bloch oscillations have been carried out in terahertz emission[19–22], electro-optic detection,[23,22] and four-wave mixing experiment.[24] Past studies have mainly been focused on one-dimensional superlattices and three-dimensional vertical quantum-well superlattice structures for theoretical simplicity and technical feasibility, while very few studies have been carried out in two dimensional (2D) systems. Recently, 2D systems with patterned surface structures have been studied for various advantages.[18]

In this paper, we study theoretically the nonlinear DC current of a degenerate electron gas in a 2D structure, which is modulated through surface patterning in the direction of the field. The dependences of the current on the field, the electron density and the temperature are investigated. Our model is introduced with a goal toward understanding recent data from a 2D quantum well (QW) with a periodically modulated potential to be introduced later.[18] A relaxation-time approximation[11,16] is employed for inelastic scattering, while impurity scattering is considered microscopically. The role of elastic and inelastic scattering on the nonlinear current is studied. The result is applied to the Kronig-Penney model and is compared with our recent data from a modulated 2D GaAs QW. It is found theoretically that, for a given total scattering rate, the field dependence of the current is insensitive to the ratio of the elastic and inelastic scattering rates in contrast with the recent results of the nonlinear current of similar models of a single mini-band in one dimension and three

dimensions, where the current depends sensitively on the ratio of the two scattering rates for a fixed total scattering rate.

The organization of the paper is as follows. A basic formalism is presented in the next Section. In Sec. III, the model is evaluated exactly for a single parabolic band. A numerical evaluation of the results for the Kronig-Penney model as well as a comparison with recent data is given in Sec. IV. A brief summary of the results is presented in Sec. V.

II. BASIC FORMALISM

The steady-state Boltzmann equation is given, in a relaxation-time approximation,[11,16] by

$$-\frac{eF}{\hbar}\frac{\partial f_n(\mathbf{k})}{\partial k_x} = -\nu_{in}[f_n(\mathbf{k}) - f^{(0)}(\varepsilon_{n,\mathbf{k}})]$$
$$+\frac{2\pi}{\hbar}\sum_{n',\mathbf{k}'}|U_{n\mathbf{k},n'\mathbf{k}'}|^2\delta(\varepsilon_{n\mathbf{k}} - \varepsilon_{n'\mathbf{k}'})\{f_{n'}(\mathbf{k}') - f_n(\mathbf{k})\}, \tag{1}$$

where ν_{in} is the inelastic scattering rate assumed to be a constant, U denotes elastic scattering, n is the band index, $\mathbf{k}$ is the wave vector, $f^{(0)}(\varepsilon)$ is the Fermi function, and $f_n(\mathbf{k})$ is the nonequilibrium distribution function. The energy is given by

$$\varepsilon_{n,\mathbf{k}} \equiv \varepsilon_n(k_x,k_y) = \varepsilon_\perp(k_y) + \varepsilon_n(k_x);\ \varepsilon_n(x) = -\sum_{m=0}^{\infty} t_{n,m}\cos mx, \tag{2}$$

where $\varepsilon_\perp(k_y) = \hbar^2k_y^2/2m^*, m^*$ is the effective mass and $-\pi \le x \equiv pk_x \le \pi$. The band energy $\varepsilon_n(k_x)$ is generated by the potential-energy modulation in the x direction which is also the direction of the field F. The quantity $t_{n,m}$ is a Fourier coefficient. Equation (1) includes interband scattering and ignores interband tunneling.

In order to simplify the problem at this point, we assume that $\tilde{D} = \hbar/\pi|U_{n\mathbf{k},n'\mathbf{k}'}|^2$ is a constant, relevant to a short-range potential and rewrite Eq. (1) as

$$-\frac{eF}{\hbar}\frac{\partial f_n(\mathbf{k})}{\partial k_x} = -\nu_{in}(f_n(\mathbf{k}) - f^{(0)}(\varepsilon_{n,\mathbf{k}})) - \frac{2}{\tilde{D}}\sum_{n',\mathbf{k}'}[f_n(\mathbf{k}) - f_{n'}(\mathbf{k}')]\delta(\varepsilon_{n,\mathbf{k}} - \varepsilon_{n',\mathbf{k}'}). \tag{3}$$

We mention here that a different assumption $\tilde{D} = D(\varepsilon_{n,\mathbf{k}})/\nu_e$, namely $|U_{n\mathbf{k},n'\mathbf{k}'}|^2 = \hbar\nu_e/\pi D(\varepsilon_{n,\mathbf{k}})$ with a constant elastic scattering rate ν_e was introduced in an earlier treatment by Gerhardts for a three dimensional system with a single tight-binding band in the

direction of the potential modulation to make the problem more tractable.[11] Here, $D(\varepsilon)$ is the density of states (DOS).

We define

$$\nu(\varepsilon) = \nu_{in} + \nu_{el}(\varepsilon),\ \nu_{el}(\varepsilon) = D(\varepsilon)/\tilde{D} \tag{4}$$

$$h(\varepsilon) = \frac{2}{\tilde{D}} \sum_{n',\mathbf{k}'} f_{n'}(\mathbf{k}')\delta(\varepsilon - \varepsilon_{n',\mathbf{k}'}) \tag{5}$$

and recast Eq. (3) into[11]

$$-\frac{peF}{\hbar}\frac{\partial f_n(\mathbf{k})}{\partial x} = -\nu(\varepsilon_{n,\mathbf{k}})f_n(\mathbf{k}) + \nu_{in}f^{(0)}(\varepsilon_{n,\mathbf{k}}) + h(\varepsilon_{n,\mathbf{k}}). \tag{6}$$

Note that Eq. (6) conserves the number of particles. Following Gerhardts[11], we introduce a quantity $\phi_n(\mathbf{k})$ by

$$f_n(\mathbf{k}) = \phi_n(\mathbf{k}) \exp[\frac{\hbar}{peF}\int_0^x \nu(\varepsilon_n(k'_x, k_y))dx']. \tag{7}$$

Defining $\gamma_{in} = peF/\hbar\nu_{in}$, and inserting in Eq. (6), we find

$$\phi_n(\mathbf{k}) = \int_x^\infty \tilde{G}(\varepsilon_n(k'_x, k_y)) \exp[-\frac{\hbar}{peF}\int_0^{x'} \nu(\varepsilon_n(k''_x, k_y))dx'']dx', \tag{8}$$

where $x' = pk'_x$, *etc*, and

$$\tilde{G}(\varepsilon) = \gamma_{in}^{-1} f^{(0)}(\varepsilon) + \frac{\hbar}{peF}h(\varepsilon). \tag{9}$$

The quantity $f_n(\mathbf{k})$ is then given by

$$f_n(\mathbf{k}) = \int_0^\infty \tilde{G}(\varepsilon_n(k_x + k'_x, k_y)) \exp[-\frac{\hbar}{peF}\int_0^{x'} \nu(\varepsilon_n(k_x + k''_x, k_y))dx'']dx'. \tag{10}$$

Inserting Eq. (10) in Eq. (9), we find in view of Eq. (5)

$$\tilde{G}(\varepsilon) = \frac{f^{(0)}(\varepsilon)}{\gamma_{in}} + \frac{2}{\gamma_{e\mu}D(\mu)}\sum_{n,\mathbf{k}} \delta(\varepsilon - \varepsilon_{n,\mathbf{k}})$$
$$\times \int_0^\infty \tilde{G}(\varepsilon_n(k_x + k'_x, k_y)) \exp[-\frac{\hbar}{peF}\int_0^{x'} \nu(\varepsilon_n(k_x + k''_x, k_y))dx'']dx', \tag{11}$$

where $\tilde{D} = D(\mu)/\nu_{el}(\mu)$ from Eq. (4), μ is the chemical potential, $\gamma_{e\mu} = peF/\hbar\nu_{e\mu}$, and $\nu_{e\mu} = \nu_{el}(\mu)$. The current density is given by

$$j_{2D} = -\frac{2ep}{\hbar S}\sum_{n,m,\mathbf{k}} t_{n,m} m \sin(x) f_n(\mathbf{k}), \tag{12}$$

where S is the area of the sample.

III. SINGLE PARABOLIC BAND

Here, we show that the present model can be evaluated exactly for a single parabolic band in the x direction $\varepsilon_n(k_x) = \hbar^2 k_x^2/2m^*$ in Eq. (2) and yields the result of the linear response theory for a general field. In this case, the length p in Eq. (6) is an arbitrary constant and will be chosen to be the inverse Fermi wave number $p = 1/k_F$. Also, the scattering rate $\nu = \nu_{in} + \nu_{el}$ in Eq. (4) is a constant due to the flat DOS, yielding for Eq. (10)

$$f(\mathbf{k}) = \int_0^\infty \exp(-x'/\gamma)\tilde{G}[\varepsilon_F \left(y^2 + (x+x')^2\right)]dx', \tag{13}$$

where ε_F is the Fermi energy, $x = k_x/k_F, y = k_y/k_F, \gamma = eF/k_F\hbar\nu, \gamma_{in} = eF/k_F\hbar\nu_{in}, \gamma_{el} = eF/k_F\hbar\nu_{el}$. It follows from Eqs. (5) and (9) that

$$\sum_{\mathbf{k}} \tilde{G}(\varepsilon_{\mathbf{k}}) = \gamma^{-1} \sum_{\mathbf{k}} f_{\mathbf{k}}. \tag{14}$$

The current density is given by

$$j_{2D} = -\frac{2e}{S}\sum_{\mathbf{k}} \frac{\hbar k_x}{m^*} f_{\mathbf{k}} = -\frac{2e\hbar k_F}{m^* S}\sum_{\mathbf{k}} x \int_0^\infty \exp(-x'/\gamma)\tilde{G}[\varepsilon_F \left(y^2 + (x+x')^2\right)]dx', \tag{15}$$

which yields, in view of Eq. (14), a well-known expression of the linear response theory:

$$j_{2D} = \frac{N_{2D}e^2 F\tau}{m^*},\ \tau = 1/\nu. \tag{16}$$

IV. NUMERICAL EVALUATION AND DISCUSSIONS

In this section, we evaluate the current and study possibly different effects of elastic and inelastic scattering. The result will be compared with the recent exact result of a one-dimensional model[16] and with the result of a three dimensional model.[11] Also, a comparison will be made with the data from a 2D GaAs QW with a patterned potential-energy structure.[18]

A. Iterative Solution

The quantity $\tilde{G}(\varepsilon)$ in Eq. (11) can be solved by iteration starting from the zeroth-order solution

$$\tilde{G}(\varepsilon) = f^{(0)}(\varepsilon)/\gamma_{in}.$$

We rewrite Eq. (11) as

$$\tilde{G}(\varepsilon) = \frac{f^{(0)}(\varepsilon)}{\gamma_{in}} + \frac{2}{\gamma_{e\mu} D(\mu)} \sum_{n,\mathbf{k}} \delta(\varepsilon - \varepsilon_{n,\mathbf{k}}) \int_0^\infty \tilde{G}(\varepsilon + \varepsilon_n(k_x + k_x') - \varepsilon_n(k_x))$$
$$\times \exp[-\frac{x'}{\gamma_{in}} - \frac{1}{\gamma_{e\mu}\Lambda(\mu)} \int_0^{x'} \Lambda(\varepsilon + \varepsilon_n(k_x + k_x'') - \varepsilon_n(k_x)) dx'']dx', \tag{17}$$

where $\Lambda(\varepsilon)$ is related to the DOS through the relationship

$$D(\varepsilon) = \frac{S\sqrt{2m^*}}{\pi^2\hbar p}\Lambda(\varepsilon) : \Lambda(\varepsilon) \equiv \sum_n \int_0^\pi \frac{\theta(\varepsilon - \varepsilon_n(x))}{\sqrt{\varepsilon - \varepsilon_n(x)}} dx. \tag{18}$$

Here, $\theta(\varepsilon)$ is a unit step function.

The electric field is represented as a dimensionless quantity $\mathcal{F} = F/F^*$, where

$$F^* = \frac{\hbar\nu_\mu}{ep},\ \nu_\mu = \nu_{in} + \nu_{e\mu}, \tag{19}$$

yielding

$$\gamma_{in} = \mathcal{F}(1 + R^{-1}),\ \gamma_{e\mu} = \mathcal{F}(1 + R), \tag{20}$$

where $R = \nu_{in}/\nu_{e\mu}$. The quantities ν_μ and R will be employed as variables which determine F^*, γ_{in}, and $\gamma_{e\mu}$ for a given field. Note that $F = F^*$ corresponds to a special field where $\omega_F/\nu_{e\mu} = \omega_F\tau_{e\mu} = 1$ and is therefore roughly the threshold field where the Bloch oscillation completes $1/2\pi$ of a cycle before the electrons are scattered. It can rigorously be shown from Eqs. Eq. (10) - (12) that the current density vanishes asymptotically as $j_{2D} \propto 1/\mathcal{F}$ in the limit $\mathcal{F} \gg 1$ as also will be demonstrated numerically later.

It is convenient to split the sum over the band index in Eq. (13) into the sum $\sum_{n=high}$ over the extended states with large energy-dispersion and the sum $\sum_{n=low}$ over the low-lying-energy states (*e.g.,* bound states below the barrier) with negligible dispersion. For the latter

contribution, the x', x'' integrations in Eq. (13) can immediately be carried out yielding

$$\tilde{G}(\varepsilon) = F(\varepsilon)^{-1}\left[\frac{f^{(0)}(\varepsilon)}{\gamma_{in}} + \frac{1}{2\gamma_{eF}\Lambda(\mu)}\sum_{n=high}\int_{-\pi}^{\pi} dx\ \frac{\theta(\varepsilon-\varepsilon_n(x))}{\sqrt{\varepsilon-\varepsilon_n(x)}}\int_0^{\infty} dx'\right.$$

$$\left.\times\tilde{G}(\varepsilon+\varepsilon_n(x+x')-\varepsilon_n(x))\exp\left(-[\frac{x'}{\gamma_{in}} + \frac{1}{\gamma_{e\mu}\Lambda(\mu)}\int_0^{x'} dx''\ \Lambda(\varepsilon+\varepsilon_n(x+x'')-\varepsilon_n(x))]\right)\right], \tag{21}$$

where

$$F(\varepsilon) = \frac{\gamma_{e\mu}/\gamma_{in} + [\Lambda(\varepsilon) - \Lambda_{\rm low}(\varepsilon)]/\Lambda(\mu)}{\gamma_{e\mu}/\gamma_{in} + \Lambda(\varepsilon)/\Lambda(\mu)} \tag{22}$$

and

$$\Lambda_{\rm low}(\varepsilon) = \pi\sum_{n=\rm low}\frac{\theta(\varepsilon-\varepsilon_n(x))}{\sqrt{\varepsilon-\varepsilon_n(x)}}. \tag{23}$$

It is seen that $0 < F(\varepsilon) < 1$. Also, we rewrite Eq. (10) as

$$f_n(\mathbf{k}) = \int_0^{\infty}\tilde{G}(\varepsilon_n(k_x+k'_x,k_y))\exp\left(-[\frac{x'}{\gamma_{in}} + \frac{1}{\gamma_{e\mu}\Lambda(\mu)}\int_0^{x'}\Lambda(\varepsilon_n(k_x+k''_x,k_y))dx'']\right)dx'. \tag{24}$$

B. Numerical Results and Comparison with Data

In the following, we apply our result to a 2D GaAs QW which has a modulated potential along the direction of the field according to the Kronig-Penney model with a valley width $a = 150$ nm, a barrier width $b = 200$ nm, a superlattice period $p = a + b$, a barrier height $V_0 = 1$ meV, and an effective mass $m^* = 0.067m_0$. Here, m_0 is the free-electron mass. In this case, we find $F^* \simeq 1.88\nu_\mu \times 10^{-11}$ Vsec/cm from Eq. (15). The role of the total scattering rate ν_μ is to set the scale of the field through F^*. For the low-lying energy states $n = low$ in Eq. (23), we include the two bound states at $\varepsilon = 0.1418$ meV, $\varepsilon = 0.54268$ meV below the barrier. The coefficients $t_{n,m}$ in Eqs. (12) are obtained by a Fourier expansion for each band. It was found that only a few cosine components are necessary to fit the numerical data for energy dispersion.

Figure 1 displays the current density as a function of the reduced field $\mathcal{F}$ for several values of $R = 0.1$ (thick black solid curve), $R = 1$ (red dashed curve), and $R = 100$ (thin green solid curve) at 4 K for $N_{2D} = 2.2 \times 10^{11}/\text{cm}^{\ 2}$ (upper curves) and $N_{2D} = 10^{11}/\text{cm}^2$ (lower curves). For $\nu_\mu = 10^{11}/\text{sec}$ at 4 K relevant, for example, corresponding to the sample mobility $\sim 0.3 \times 10^6$ cm^2/Vsec, we estimate $F^*_{4K} \simeq 1.88$ V/cm. This field is much smaller than that in the previously studied regular superlattices mainly due to the large superlattice period in Eq. (19) in our structure. In superlattices with a short period, conduction occurs in the mini-bands below the barrier, while electrons flow in the bands above the barrier in our structure with a wide barrier. The magnitude of the field at the peak current remained approximately at $F \simeq F^*$ when the energy gaps between the above-barrier bands are increased by changing the well depth from $V_0 = 1$ meV to $V_0 = 3$ meV. The blue dashed-doted curves show the asymptotic behavior of the current $\propto 1/F$. The peak current occurs near $F \simeq F^*$ *i.e.,* $\omega_F \tau_\mu \simeq 1$ in all cases. As expected, the current rises slowly in Fig. 1 with increasing R because inelastic scattering is not as efficient as elastic scattering for momentum relaxation. However, the field dependence of the current is not very sensitive to the ratio R in a striking contrast to the results of single-band models of one dimensional superlattice[16,26] and three-dimensional system[11] based on the similar relaxation-time approximation, where it is very sensitive to R.

In order to see how the current evolves with the temperature T starting from a low temperature $T_0 = 4$ K, we assume that the low-temperature elastic scattering rate ν_{el} is insensitive to the temperature, while the electron-phonon scattering rate $\nu_{in}(T) \propto T$ is proportional to the temperature. The latter is due to the fact that momentum relaxation through acoustic-phonon scattering arises from scattering in the thermal layer of the Fermi surface by phonons with a maximum energy $k_B T_{B-G}$ corresponding to the wave length $\sim 2k_F$. In the current system with $N_{2D} = 2.2 \times 10^{11}/cm^2$, the Fermi wave numbers k_F is small, yielding a small Bloch-Grüneisen temperature $T_{B-G} \sim 5$ K.[27] The scattering rate becomes linear above this temperature, while showing rapid Bloch-Grüneisen decrease (increase) of the scattering rate (mobility) below this temperature as observed by Stormer et al.[27] We

therefore estimate $R_T \simeq (T/T_0)R_{T_0}, F_T^* = F_{T_0}^*[(T/T_{T_0})R_{T_0}+1]/(R_{T_0}+1)$, yielding, for example, $R_{20K} \simeq 5R_{4K}, F_{20K}^* = F_{4K}^*(5R_{4K}+1)/(R_{4K}+1)$. Here, R_{4K} is the ratio of the inelastic and elastic scattering rates at 4 K employed in Fig. 1. Another contribution to the temperature-dependence of the current enters through chemical potential and Fermi function in Eq. (17). In Fig. 2, we compare the current vs. F shown in Fig. 1 at 4 K with the field dependence of the current at 20 K. The thick black solid (dashed) curve represents the current at 4 K (20 K) for the case $R_{4K} = 0.1$ ($R_{20K} = 5R_{4K} = 0.5$), while the thin red solid (dashed) curve displays the current at 4 K (20 K) for the case $R_{4K} = 1$ ($R_{20K} = 5R_{4K} = 5$). The field is in units of $F_{4K}^* \simeq 0.188$ V/cm. It is seen that while the peak current decreases very slowly with T, the peak shifts to a higher field at $T = 20$ K and the width of the peak broadens significantly. It should be pointed out here that the field dependence of the current at $T = 20$ K looks very different for $R = 0.5$ and $R = 5$ because the total scattering rates are different for these two cases. For a fixed total scattering rate, the two concomitant curves will look similar to those shown for $T = 4$ K in Fig. 2 with somewhat reduced peaks. The asymptotic behavior of the current density $j_{2D} \propto 1/F$ obtains at higher fields.

The present numerical study based on the Kronig-Penney model was initiated with a goal toward understanding our recent high-field data from a 2D GaAs QW structure with a periodically modulated surface potential.[18] In this system, a 2D periodic metal grid was fabricated on a surface above a high-mobility ($> 10^6$ cm^2/Vsec) GaAs QW with a regular square array of holes of diameter $a = 150$ nm with a period $a + b = 350$ nm in x and y directions. The depression of the potential energy under the holes is about $V_0 = 1$ meV. The sample mobility is reduced after patterning. We apply the Kronig-Penney model to this structure with the applied field in the x direction, ignoring the potential modulation in the perpendicular direction. This periodic modulation of the potential opens small gaps of a fraction of an meV. The above parameters as well as the total scattering rate at 4 K and the density $N_{2D} = 2.2 \times 10^{11}$ cm^{-2} to be used for the numerical fit below are the same as those employed for the studies presented in Figs. 1 and 2 above. The plot of the current I_{sd} vs. the source-drain voltage V_{sd} for the field F is obtained according to

$$I_{sd} = \ell_\perp j_{2D}(\mathcal{F}),\ V_{sd} = R_c I_{sd} + \ell_\parallel \mathcal{F} F^*, \tag{25}$$

where $\ell_\perp = 0.2$ mm is the cross section of the sample (smaller than $\ell_\perp = 0.7$ mm estimated for Sample B in Ref.[18]), $R_c = 1.16$ kΩ is the contact resistance and $\ell_\parallel = 1.5$ mm is the length of the sample along the current direction[18] for $\tau = 0.029\times10^{-10}$ sec [or, alternatively, $\ell_\parallel = 5.2$ mm for $\tau = 10^{-11}$ sec]. In Fig. 3, we compare the data (thick black dashed curve) for the current as a function of the source-drain voltage with the curves generated for $R = 100$ (thick black solid curve) and $R = 0.2$ (thin red dashed-dotted curve). The thin blue solid curve shows the effect of including the field-induced electron-phonon scattering rate for $R = 1$ to be discussed below.

The field-free $\nu_{in} = \nu_{in}^{(0)}$ arises from electron-phonon scattering inside the thermal layer of the Fermi surface. Additional contribution to ν_{in} arises when the field-induced displacement of the Fermi surface creates empty phase space into which electrons can fall through electron-phonon interaction, increasing ν_{in} with F and thereby the scaling factor F^*. According to the results presented in Figs. 1 and 2, the net effect is to increase the scale of F on the horizontal axis through F^* and stretch the curves to the right and flatten them when the current density is plotted against F.[28] This effect is clearly seen by the thin blue dotted curve in Fig. 3 which brings the theoretical curve closer to the data. It may be possible that higher-order effects of F to ν_{in} above the threshold field of the negative conductance regime can make the current flatter as shown by the data beyond 4 Volt and the thin blue solid curve to be discussed below.

In order to quantify the above discussion, we estimate the total scattering rate $\nu = 1/\tau = \nu_{in} + \nu_{e\mu}$ that includes the effect of the field-induced relaxation rate for ν_{in} in the following. As mentioned above, the additional field-induced contribution to ν_{in} arises from the field-induced displacement $\propto F\tau$ of the Fermi surface and is given by

$$\tau_{in}^0 \nu_{in} = \frac{\tau_{in}^0}{\tau_{in}} = 1 + A(F)\frac{F}{F_0}\frac{\tau}{\tau_0}, \tag{26}$$

where $\nu_{in} = 1/\tau_{in}, \nu_{in}^{(0)} = 1/\tau_{in}^0, \nu_0 = 1/\tau_0 = \nu_{in}^{(0)} + \nu_{e\mu}$ and F_0 is a field constant to be determined microscopically from electron-phonon scattering. The indeces "0" signify field-

free quantities. The second term in Eq. (26) is proportional to the total displacement of the Fermi surface during the effective scattering time τ. The quantity $A(F) = 1$ for a small field F in the linear regime but can become larger $A(F) > 1$ at large fields due to higher-order effects, whereby all electrons inside the original Fermi surface can relax through rapid phonon emission. Equation (26) yields

$$\frac{1}{\tau} = \frac{1}{2\tau_0}\left(1 + \sqrt{1 + \frac{4A(F)F}{\alpha_R F_0}}\right), \tag{27}$$

where $\alpha_R = (1+R)/R$ and $R = \nu_{in}^{(0)}/\nu_{e\mu}$ as defined earlier.

The constant F_0 is determined from the low-field numerical estimate:

$$\nu_{in} = \nu_{in}^0 + sF \times 10^{10}\ \mathrm{sec}^{-1}, \tag{28}$$

where F is in units of Volt/cm and $s \simeq 0.32$ for appropriate phonon parameters for GaAs.[30] Comparing Eqs. (27) and (28) for small F, we find $F_0 = 1/[s\alpha_R\tau_0 \times 10^{10}]$ Vsec/cm. The field-dependent $\nu = 1/\tau$ in Eq. (27) with $A = 1$ is then employed for the field scale factor F^* for the thin blue dotted curve in Fig. 3 using $R = 1$. The thin blue solid curve therein is obtained by employing a simple function

$$A(F) = 1 + 1.5\theta(F - 1.7F^*). \tag{29}$$

The fit to the data can be made smoother by using a more gradual transition for the step function in the second term in in Eq. (29).

V. CONCLUSIONS

We studied the nonlinear response of the current of a 2D electron gas with a periodically modulated potential in the direction of a strong DC electric field at low temperatures employing the Kronig-Penney model. The dependence of the current on the field, the electron density and the temperature was investigated by using a relaxation-time approximation for inelastic scattering, while considering impurity scattering microscopically. The roles of elastic and inelastic scattering on the nonlinear current were examined. It is found that the

current depends roughly only on the total scattering rate in contrast with the recent results of the nonlinear current of single-band models based on similar relaxation-time approximation in one dimension[16] and three dimensions.[11] We believe this behavior is due to the two dimensionality of the present system with multiple bands arising from uni-directional modulation of the potential energy in the field direction combined with free motion in the transverse direction. A similar relaxation-time model with a single tight-binding band in the field direction and free motion in the transverse direction is under study. A preliminary result indicates that the reduced field at the peak current depends sensitively on the ratio of the inelastic and elastic scattering rates in contrast with the behavior shown in Fig. 1. The theoretical result of this paper is favorably compared with our recent data. We demonstrated that agreement with the data improves when the effect of the field on the relaxation rate is included.

We have studied transport in a two-dimensional gas, while past studies deal with an electron gas in one or three dimensions. A more important distinction is that previously studied structures have a short lattice period and deep quantum wells, where conduction occurs in the mini-bands below the barrier. In contrast, our sample has a large period with wide barriers and shallow wells. The electrons flow in the bands above the barrier. As a result, the peak current and thus the negative differential conductance occur at a much smaller field in our sample compared to the regular superlattices due to a larger lattice period. In our sample, the levels below the barrier are localized and do not carry current. However, they can still affect the current owing to the fact that electrons are scattered into and out of these states in our model in the transverse direction, where free electron motion is assumed.

A key approximation employed for our model is the relaxation-time approximation for inelastic scattering. This approximation is known to yield qualitative agreement with the results from microscopic theories in one dimension[16,17] and three dimensions.[11,9] A second important assumption made in our model is the neglect of interband (*i.e.,* Zener) tunneling. This assumption is valid only when the tunneling probability is small at the band edges. A

rough estimate of this probability is given by[29] $P = \exp(-A)$, where $Q \simeq \varepsilon_{gap}^2/(4\varepsilon_p epF), \varepsilon_p = \hbar^2/2m^*p^2$, and ε_{gap} is the gap energy. Assuming that $\varepsilon_{gap} \equiv \varepsilon_0$ yields $Q = 1$, interband tunneling will be negligible in the limit $Q \gg 1$, namely $\varepsilon_{gap} \gg \varepsilon_0$. We estimate $\varepsilon_0 = 0.077$ meV for our sample parameters for $F = 1$ V/cm. The numerical gaps generated for our sample for the small modulation amplitude $V_0 = 1$ meV are of the order of this magnitude or somewhat larger and do not satisfy $P \ll 1$. The gap sizes increase by a factor of $2 \sim 3$ for $V_0 = 3$ meV. In a stringent sense, the current model will be applicable to a system with a larger modulation amplitude $V_0 \gg 1$ meV. However, the data in Fig. 3 clearly show high-field negative conductance behavior indicative of Bloch oscillations.

ACKNOWLEDGMENTS

This work was supported by DOE/BES at Sandia National Laboratories. Sandia is a multiprogram laboratory operated by Sandia Corporation, a Lockheed Martin Company, for the U.S. DOE under Contract No.DE-AC04-94AL85000.

†: Present address

REFERENCES

[1] F. Bloch, Z. Phys. **52**, 555 (1928).

[2] L. Esaki and R. Tsu, IBM J. Res. Dev. **14**, 61 (1970).

[3] S. A. Ktitorov, G. S. Simin, and V. Ya. Sindalovskii, Sov. Phys. Solid State **13**, 1872 (1972).

[4] F. G. Bass and E. A. Rubinshtein, Fiz. Tverd. Tela Lenningrad **19**, 1379 (1977) [Sov. Phys. Solid Sate **19**, 800 (1977)].

[5] R. A. Suris and Shchamkhalova, Fiz. Tekh. Poluprovodn. **18**, 1178 (1984) [Sov. Phys. Semicond. **18**, 738 (1984)].

[6] M. Artaki and K. Hess, Superlatt. Microstruct. **1**, 489 (1985).

[7] A. Sibille, J. F. Palmier, H. Wang, and F. Mollot, Phys. Rev. Lett. **64**, 52 (1990).

[8] H. T. Grahn, K. von Klitzing, K. Ploog, and G. H. Dőhler, Phys. Rev. B **43**, 12094 (1991).

[9] X. L. Lei, N. J. M. Horing, and H. L. Cui, Phys. Rev. Lett. **66**, 3277 (1991).

[10] A. A. Ignatov, E. P. Dodin, and V. I. Shashkin, Mod. Phys. Lett. B **5**, 1087 (1991).

[11] R. R. Gerhardts, Phys. Rev. B **48**, 9178 (1993).

[12] A. A. Ignatov, K. F. Renk, and E. P. Dodin, Phys. Rev. Lett. **70**, 1996 (1993).

[13] S. Rott, P. Binder, N. Linder, and G. H. Döhler, Phys. Rev. B **59**, 7334 (1999).

[14] F. Löser, Yu. A. Kosevich, K. Köhler, and K. Leo, Phys. Rev. B **61**, R13373 (2000).

[15] Yu. A. Kosevich, Phys. Rev. B **63**, 205313 (2001).

[16] S. K. Lyo, Phys. Rev. B **77**, 195306 (2008).

[17] D. Huang, S. K. Lyo, and G. Gumbs, Phys. Rev. B **79**, 155308 (2009).

[18] W. Pan, S. K. Lyo, J. L. Reno, J. A. Simmons, D. Li and S. R. J. Brueck, Appl. Phys.

Lett. **92**, 052104 (2008).

[19] C. Waschke, H. G. Roskos, R. Schwedler, K. Leo, H. Kurz, and K. Köhler, Phys. Rev. Lett. **70**, 3319 (1993).

[20] R. Martini, G. Klose, H. G. Roskos, H. Kurz, H. T. Grahn, and R. Hey, Phys. Rev. B **54**, R14325 (1996).

[21] K. Jin, M. Odnoblyudov, Y. Shimada, K. Hirakawa, and K. A. Chao, Phys. Rev. B **68**, 153315 (2003).

[22] N. Sekine and K. Hirakawa, Phys. Rev. Lett. **94**, 057408 (2005).

[23] M. Först, G. Segschneider, T. Dekorsy, H. Kurz, and K. Köhler, Phys. Rev. B **61**, R10563 (2000).

[24] V. G. Lyssenko, G. Valusis, F. Löser, T. Hasche, K. Leo, M. M. Dignam, and K. Köhler, Phys. Rev. Lett. **79**, 301 (1997)

[25] S. Rott, N. Linder, and G. H. Döhler, Phys. Rev. B **65**, 195301 (2002) and references therein.

[26] In the exact treatment of the one-dimensional superlattice by the author[16], the the peak current increases by 70 % when the rates $\nu_{in} = 5 \times 10^{10}, \nu_{el} = 10^{11}$ sec^{-1} with $R = 0.5$ for the total scattering rate $\nu = \nu_{in} + \nu_{el} = 1.5 \times 10^{11}$ sec^{-1} are switched to $\nu_{in} = 10^{11}, \nu_{el} = 5 \times 10^{10}$ sec^{-1} with $R = 2$ as seen in Fig. 2 of Ref.[16].

[27] H. L. Stormer, L. N. Pfeiffer, K. W. Baldwin, and K. W. West, Phys. Rev. B **41**, 1278 (1990).

[28] Another smaller effect arises from changing the ratio of the inelastic to elastic scattering rates discussed earlier.

[29] *Principles of the Theory of Solids*, J. M. Ziman, p.192 [Cambridge U. Press, New York, 1979.]

[30] S. K. Lyo, Phys. Rev. B **40**, 6458 (1989).

FIGURES

FIG. 1. Current density vs. reduced field $\mathcal{F} = F/F^*$ for several values of $R = \nu_{in}/\nu_{el} = 0.1$ (thick black solid curve), $R = 1$ (red dashed curve), and $R = 100$ (thin green solid curve) for a fixed total scattering rate at 4 K for $N_{2D} = 2.2 \times 10^{11}/\text{cm}^{\,2}$ (upper curves) and $N_{2D} = 10^{11}/\text{cm}^2$ (lower curves). The scale factor F^*_{4K} can be different for the two densities. The blue dashed-dotted curves show the asymptotic behavior of the current $\propto 1/F$. Other parameters are given in the text.

FIG. 2. Field dependence of the current at two temperatures: $T = 4$ K for $R_{4K} = \nu_{in}/\nu_{el} = 0.1$ (thick black solid curve), $R_{4K} = 1$ (thick black dotted curve) with a fixed total scattering rate and at $T = 20$ K for $R_{20K} = 0.5$ (thin red dashed curve) and $R_{20K} = 5$ (thin red dashed-dotted curve), assuming that ν_{el} is insensitive to T and ν_{in} is linear in T (*e.g.*, $R_{20K} = 5R_{4K}$). The current decays as $\propto 1/F$ asymptotically. Other parameters are given in the text.

FIG. 3. The total current I vs. source-drain voltage V_{sd} for $R = 0.2$ (thick red dashed-dotted curve), and $R = 100$ (thick black solid curve), and the data (thick black dashed curve) at 4 K for $N_{2D} = 2.2 \times 10^{11}/\text{cm}^{\,2}$. The thin blue dotted and solid curves are plotted for $R = 1$ and include the effect of field-induced ν_{in} for $A(F) = 1$ and $A(F)$ given in Eq. (29), respectively. Other parameters are given in the text.

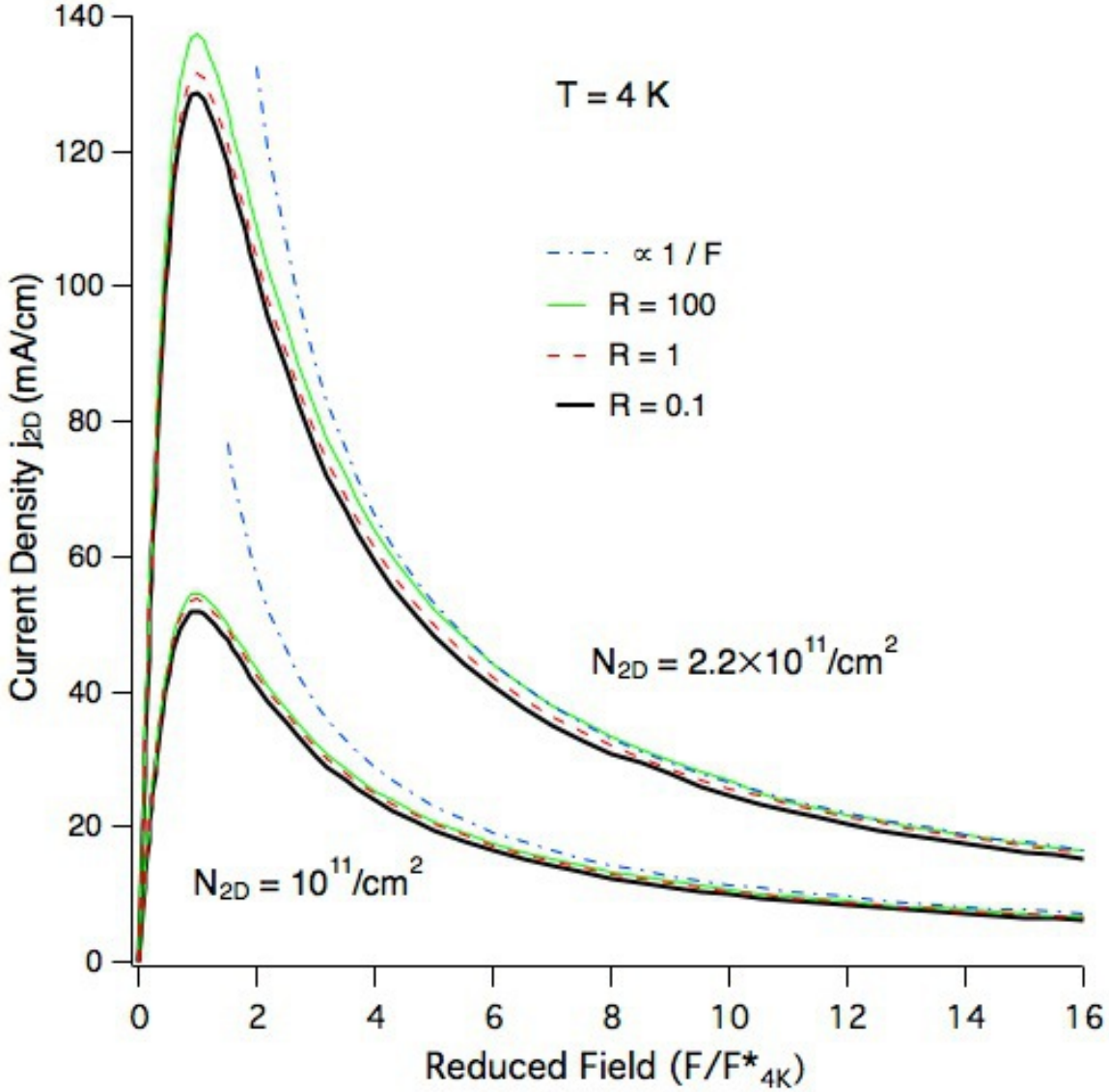
T = 4 K
∝ 1 / F
R = 100
R = 1
R = 0.1
N2D = 2.2×10^11/cm^2
N2D = 10^11/cm^2
Current Density j2D (mA/cm)
Reduced Field (F/F*4K)
0
20
40
60
80
100
120
140
0
2
4
6
8
10
12
14
16

Fig. 1

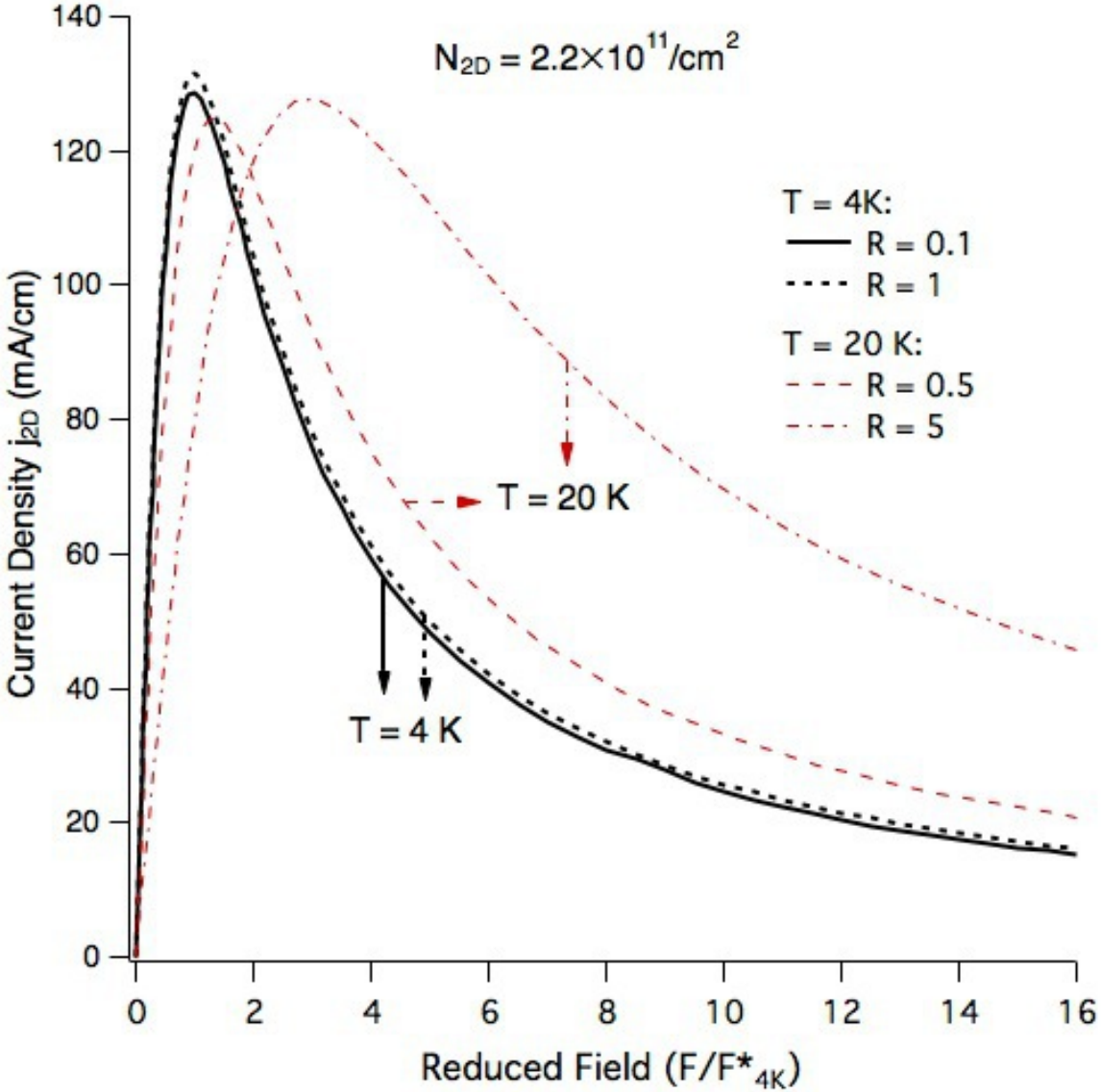
$N_{2D} = 2.2\times10^{11}/cm^2$
T = 4K:
R = 0.1
R = 1
T = 20 K:
R = 0.5
R = 5
T = 20 K
T = 4 K
Current Density j_{2D} (mA/cm)
Reduced Field (F/F^*_{4K})
0
20
40
60
80
100
120
140
0
2
4
6
8
10
12
14
16

Fig. 2

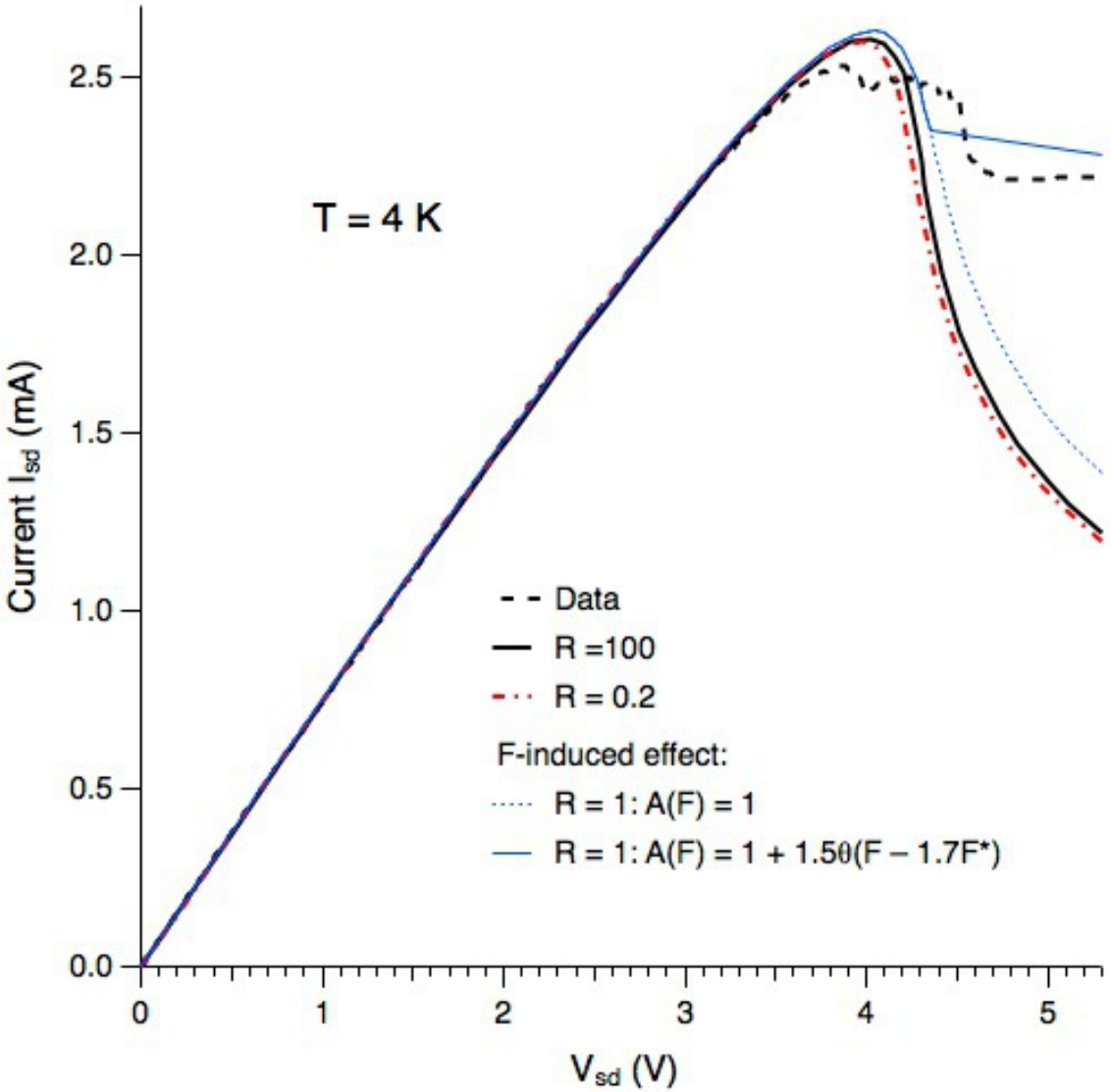
T = 4 K
Current I_{sd} (mA)
V_{sd} (V)
2.5
2.0
1.5
1.0
0.5
0.0
0
1
2
3
4
5
Data
R =100
R = 0.2
F-induced effect:
R = 1: A(F) = 1
R = 1: A(F) = 1 + 1.5θ(F – 1.7F*)

Fig. 3